Journal of Controlled Release 352 (2022) 623–636

Contents lists available at ScienceDirect

Journal of Controlled Release

journal homepage: www.elsevier.com/locate/jconrel

A Pt(IV)-conjugated brain penetrant macrocyclic peptide shows pre-clinical efficacy in glioblastoma

J.L. Jimenez-Macias [a,b,c], Y.-C. Lee [c,1], E. Miller [c], T. Finkelberg [a], M. Zdioruk [a], G. Berger [a,d], C.E. Farquhar [c], M.O. Nowicki [a], C.-F. Cho [a,e,f,i], B.I. Fedeles [g], A. Loas [c], B.L. Pentelute [c,g,h,i,*], S. E. Lawler [a,b,**]

[a] Harvey Cushing Neuro-Oncology Laboratories, Department of Neurosurgery, Brigham and Women's Hospital, Harvard Medical School, Boston, MA 02115, USA
[b] Department of Pathology and Laboratory Medicine, Legorreta Cancer Center, Brown University, Providence, RI 02903, USA
[c] Department of Chemistry, Massachusetts Institute of Technology, Cambridge, MA 02139, USA
[d] Microbiology, Bioorganic and Macromolecular Chemistry, Faculty of Pharmacy, Université Libre de Bruxelles, Brussels 1050, Belgium
[e] Program in Neuroscience, Harvard Medical School, Boston, MA 02115, USA
[f] Harvard Stem Cell Institute, Harvard University, Boston, MA 02115, USA
[g] Center for Environmental Health Sciences, Massachusetts Institute of Technology, Cambridge, MA 02139, USA
[h] The Koch Institute for Integrative Cancer Research, Massachusetts Institute of Technology, 500 Main Street, Cambridge, MA 02142, USA
[i] Broad Institute of MIT and Harvard, 415 Main Street, Cambridge, MA 02142, USA

ARTICLE INFO

Keywords:
Glioblastoma
Blood-brain barrier
Drug delivery
Cell-penetrating peptide
Platinum(IV)
Cisplatin

ABSTRACT

Glioblastoma (GBM) is the most aggressive primary malignant brain tumor, with a median survival of approximately 15 months. Treatment is limited by the blood-brain barrier (BBB) which restricts the passage of most drugs to the brain. We previously reported the design and synthesis of a BBB-penetrant macrocyclic cell-penetrating peptide conjugate (M13) covalently linked at the axial position of a Pt(IV) cisplatin prodrug. Here we show the Pt(IV)-M13 conjugate releases active cisplatin upon intracellular reduction and effects potent *in vitro* GBM cell killing. Pt(IV)-M13 significantly increased platinum uptake in an *in vitro* BBB spheroid model and intravenous administration of Pt(IV)-M13 in GBM tumor-bearing mice led to higher platinum levels in brain tissue and intratumorally compared with cisplatin. Pt(IV)-M13 administration was tolerated in naïve nude mice at higher dosage regimes than cisplatin and significantly extended survival above controls in a murine GBM xenograft model (median survival 33 days for Pt(IV)-M13 *vs* 24 days for Pt(IV) prodrug, 22.5 days for cisplatin and 22 days for control). Increased numbers of γH2AX nuclear foci, biomarkers of DNA damage, were observed in tumors of Pt(IV)-M13-treated mice, consistent with elevated platinum levels. The present work provides the first demonstration that systemic injection of a Pt(IV) complex conjugated to a brain-penetrant macrocyclic peptide can lead to increased platinum levels in the brain and extend survival in mouse GBM models, supporting further development of this approach and the utility of brain-penetrating macrocyclic peptide conjugates for delivering non-BBB penetrant drugs to the central nervous system.

1. Introduction

Brain malignancies remain some of the most lethal and clinically challenging forms of cancer. Access to the central nervous system (CNS) for many conventional systemically delivered therapeutics is limited by the blood-brain barrier (BBB) [1,2]. Physiologically, the BBB maintains brain homeostasis by regulating the access of molecules into the CNS. This highly selective permeability of the BBB blocks the passage of the great majority of pharmaceuticals of interest into the brain at effective concentrations, limiting the ability to treat brain cancer and other CNS-related diseases [3].

Patients with glioblastoma (GBM), the most frequent primary malignant CNS tumor, have a median survival of 15 months and a 5-year survival rate below 5% [4]. Standard of care treatment consists of

* Correspondence to: B.L. Pentelute, Department of Chemistry, Massachusetts Institute of Technology, Cambridge, MA 02139, USA.
** Correspondence to: S.E. Lawler, Department of Pathology and Laboratory Medicine, Legorreta Cancer Center, Brown University, Providence, RI 02903, USA.
E-mail addresses: blp@mit.edu (B.L. Pentelute), sean_lawler@brown.edu (S.E. Lawler).
[1] Present address: Department of Chemistry, National Cheng Kung University, Tainan 701, Taiwan.

https://doi.org/10.1016/j.jconrel.2022.10.051
Received 5 June 2022; Received in revised form 29 September 2022; Accepted 25 October 2022
Available online 4 November 2022

surgical tumor resection, followed by radiotherapy in combination with temozolomide (TMZ) chemotherapy. Most patients will unfortunately develop tumor recurrence within a year of diagnosis. Available cancer drugs have little impact on GBM in patients, and it is hypothesized that improving BBB penetration would be of great potential benefit by enabling higher intra-tumoral drug concentrations [5].

Novel methods to increase drug delivery to GBM include direct intraventricular injection and implantable drug release such as Gliadel wafers [6] that can be placed in the tumor resection cavity immediately after surgery. Alternatively, the BBB can be temporarily opened using hyperosmotic solutions or focused ultrasound [7–9]. On the other hand, non-invasive CNS-delivery approaches are attractive, and some are under pre-clinical investigation. These include BBB-penetrant nanoparticles, liposomal formulations and peptide-based delivery systems, including cell-penetrating peptides (CPPs) [10–13].

Drug-conjugated peptides are emerging as key pharmaceuticals in treating a range of diseases, including cancer [14]. Peptides offer the advantages of being synthetically accessible, biologically active and structurally tunable *via* modifications such as chemical conjugation and macrocyclization ("stapling"), which may enhance peptide stability and cellular permeability [15]. CPPs possess intrinsic tissue penetrating properties that make them suitable as potential carriers for existing and potential therapeutics *in vitro* and *in vivo* [16]. The use of drug-CPP conjugates in brain cancer may be relevant due to the aforementioned properties, a notion supported by preclinical studies [17,18]. Chemical modifications such as peptide macrocyclization may add further benefit for drug delivery in the GBM setting by enhancement of peptide stability and BBB penetration properties [19,20]. However, macrocyclic CPPs have not been examined in the context of brain cancer. Macrocyclization stapling chemistries, such as perfluoroarylation, have proven effective to increase peptide stability and deliver antisense oligonucleotides to cells [21].

To develop these concepts, we previously designed M13, a derivative of the CPP Transportan 10 (TP10) modified by the incorporation of a perfluoroaryl macrocycle. This modification enhances penetration in three-dimensional BBB spheroids *in vitro* and accumulation in the mouse brain parenchyma *in vivo* [22]. After conjugation to *cis*,*cis*,*trans*-[Pt$(NH_3)_2Cl_2(OH)_2$], a Pt(IV) prodrug form of cisplatin, the resulting Pt (IV)-M13 enabled platinum delivery into the brain tissue in healthy mice [23]. Cisplatin damages DNA *via* intra- or inter-strand crosslinks [24] and is widely used in the treatment of many tumor types [25]. However, cisplatin and other platinum-based compounds are not considered applicable for GBM treatment since they do not penetrate the BBB [26]. Platinum also offers the advantage of being readily detectable by inductively-coupled plasma mass spectrometry (ICP-MS), a technique which can quantitate trace amounts of metals in biological tissue [27,28]. Thus, ICP-MS represents an effective tool for assessing the biodistribution of metal-based drugs in GBM samples acquired *in vitro* and *in vivo*.

Other studies have investigated the feasibility of using platinum compounds in GBM treatment. For example, MRI-guided focused ultrasound was applied in rat F98 glioma tumors for enhancing carboplatin intra-tumoral uptake [29]. Another study showed reduced tumor burden in recurrent GBM patients treated with carboplatin delivered *via* a novel implantable catheter system [30]. A cisplatin-derived Pt(IV) prodrug was conjugated to 2-(1-methyl-1,2,3,6-tetrahydropyridin-4-yl) propenamide to target GBM mitochondria, showing promising anti-tumoral effects *in vitro* and *in vivo* [31]. Low intensity pulsed ultrasound increases carboplatin delivery across the BBB by 4.2-fold and increased survival in GBM murine models [32]. These studies collectively support that platinum agents are feasible chemotherapies that could be used in GBM treatment safely and effectively, if the challenge of delivery across the BBB can be overcome.

In this study, we investigated platinum delivery by the Pt(IV)-M13 conjugate in a BBB spheroid model *in vitro* and in the healthy brain and tumor of a murine GBM xenograft model. We show that Pt(IV)-M13 is cytotoxic to GBM cells *in vitro*. Using ICP-MS to accurately track platinum uptake *in vivo* we show enhanced uptake in the brain and tumor tissue by Pt(IV)-M13 and a significant extension of survival in GBM tumor-bearing mice. These studies reveal the applicability of perfluoroaryl macrocyclic peptides toward improved drug delivery to GBM across the BBB.

2. Materials and methods

2.1. Synthesis of Pt(IV) and Pt(IV)-M13

The platinum(IV) prodrug Pt(IV) and Pt(IV)-M13 conjugate were synthesized as previously reported [23]. Pt(IV) and Pt(IV)-M13 stock solutions were prepared at 10 mM in *N*,*N*-dimethylformamide (DMF) (Fisher Scientific). For *in vivo* studies, cisplatin was prepared at a concentration of 3.3 mM in saline solution (0.9% NaCl) and Pt(IV) and Pt (IV)-M13 were prepared at 600 μM in 2% Tween-20 (Thermo Fisher Scientific) in 1× PBS (Gibco). Control vehicle solutions were prepared with the same DMF concentration as Pt(IV)-M13 working stocks.

2.2. Cell lines and cell culture

GBM cell lines G30-LRP, G34-pCDH, GBM-X6, the patient-derived cell line BT286 and the human oligodendroglioma G9-pCDH cell line were cultured in complete Neurobasal medium (ScienCell) supplemented with 20 μg/mL of human recombinant EGF (Peprotech), 20 μg/mL of FGF-B (Peprotech), 2% B-27 supplement (Thermo Fisher Scientific), 0.1% GlutaMax (Thermo Fisher Scientific) and 0.1% penicillin/streptomycin (Thermo Fisher Scientific). Cells would form neurospheres overnight. GBM neurosphere dissociation was done using StemPro Accutase (Thermo Fisher Scientific) to obtain single cell suspensions.

Culturing of the human cerebral microvascular endothelial cell/D3 (HCMEC/D3) cell line, human primary astrocyte cells and human primary pericyte cells was performed as reported previously [33]. For experiments, HCMEC/D3 cells were used before passage 35, primary astrocytes before passage 10 and primary pericytes before passage 8. All cell lines were cultured in T-75 vented-cap flasks (Sarsted AG and Co.) and under 5% CO_2, 95% environment air at 37 °C. Testing for mycoplasma was done with the Hot Start *Taq* 2× master mix (New England Biolabs) and STR profiling was performed by the Molecular Diagnostics laboratory at the Dana Farber Cancer Institute.

2.3. Dextran permeability assay for BBB spheroid integrity

BBB spheroids were made as previously described [33,34]. Either cisplatin, Pt(IV) or Pt(IV)-M13 was added to individual BBB spheroids and co-incubated with 10 μL/mL TRITC-dextran (155 kDa) (Sigma-Aldrich) and 1:1000 of Hoechst 33342 (Thermo Fisher Scientific) in BBB media under rotation at 37 °C for 3 h. Spheroids were washed three-times with 1× Dulbecco's PBS (Thermo Fisher Scientific) and transferred to 8-well chamber (Nunc Lab-Tek II) slides with cover-glass. Fluorescence intensity of FITC signal at 85 μm to the core of the spheroid was visualized under confocal microscopy and quantified by ImageJ (NIH and University of Wisconsin). Mean fluorescence intensity of replicates was calculated and plotted.

2.4. Cell viability assays

For addressing Pt(IV)-M13 cytotoxicity, we plated and incubated overnight 1500 individual cells/well in F-bottom black-chimney 96-well plates (Costar) in Neurobasal medium and incubated overnight. Next, cells were treated with serial dilutions of each platinum compound. After 96 h incubation, cell viability was assessed using the Cell-Titer Glo 3D reagent (Promega). Luminescence was measured in a Perkin Elmer 1450 MicroBeta TriLux Microplate Scintillation Luminescence Counter.

2.5. Growth-in-low-attachment (GILA) assay

For studying GBM sphere formation *in vitro*, GFP expressing GBM cells were plated at 2000 cells/well in ultra-low attachment 96-well plates (Costar) using 100 μL of Neurobasal medium. After 24 h of incubation, we added compounds at indicated concentrations in an additional 100 μL of neurobasal media. Plates were spun down at 1200 rpm for 3 min and fluorescence visualized using a Nikon Eclipse Ti100 microscope, and sphere diameter was measured using ImageJ software. Visualization was performed at baseline and 4 days after compound addition.

2.6. Liquid chromatography-mass spectrometry (LC-MS) analysis of Pt (IV)-M13 reduction

Sodium ascorbate in phosphate buffer (30 μL, 5 mM) and 1.5 μL of tetrabutylammonium chloride in phosphate buffer (250 μg/mL) were added to a 470 μL solution of Pt(IV)-M13 (11.6 μM) in phosphate buffer (pH 8.1) and incubated at 37 °C. Aliquots of 15 μL were removed and quenched with 15 μL of a 0.1% TFA solution in 1:1 MeCN:H_2O and subjected to LC-MS analysis after 0, 1, 2, 4, and 6 h of incubation. Peptide concentrations at different time points were quantified by integration of the total ion current (TIC) chromatogram relative to the tetrabutyl ammonium internal standard.

2.7. Inductively-coupled plasma mass spectrometry (ICP-MS)

For platinum quantitation, ICP-MS was performed using an Agilent 7900 ICP mass spectrometer, and controlled using the ICP-MS MassHunter software. Machine calibration was performed using a tuning solution (Agilent), containing 1 ng/mL (1 ppb) of Li, Co, Y, Ce and Ti trace-metals. In each experiment, the desired internal standard was added to each sample and standard solution. Standard curves were prepared with potassium tetrachloroplatinate(II) (Thermo Fisher) by generating dilutions of 0.1, 1, 10, 50, 100 and 1000 parts per billion (ppb). Isotopes selected for platinum detection were ^{195}Pt. Performance reports were registered daily for calibration and accuracy records.

2.8. Quantitation of platinum levels in vitro

For platinum detection *in vitro*, BBB spheroids were collected in 1.5 mL microcentrifuge tubes after 48–72 h of growth, and incubated with either platinum compound of interest in 1 mL of BBB medium for 3 h under rotation at 37 °C. Next, spheroids were washed three times with 1× DPBS and digested in 99.99% trace-metal free 70% HNO_3 (Bean Town Chemical) for 1 h at 65 °C. Samples were then diluted to 2% HNO_3 and submitted for ICP-MS platinum screening.

For platinum detection in GBM cells *in vitro*, G30-LRP cells and G34-pCDH cells were plated at 200,000 cells/well, left to grow for 24 h, and treated with 2 μM and 5 μM, respectively, of either cisplatin, Pt(IV) or Pt (IV)-M13 and incubated for 20 min and 2, 4, 8, 12, 24 and 48 h. Next, cells were washed 3 times with 1× PBS and digested in 70% HNO_3 for 1 h at 65 °C. Samples were then diluted to 2% HNO_3 and submitted for ICP-MS ^{195}Pt analysis.

2.9. Platinum quantitation in vivo

For detection of platinum in tissue, mice were injected with compounds at the indicated doses in 100 μL of solution *via* tail-vein injection. For organ collection, mice were euthanized *via* CO_2 inhalation. Blood perfusion was performed intracardially by infusing 1× PBS, followed by organ collection. Approximately 50 mg of organ tissue was weighed and placed in a 1.5 mL Eppendorf tube with 70% HNO_3. Tissue digestion was done by incubation for 1 h at 65 °C. Samples were diluted to 2% HNO_3 and submitted for ICP-MS platinum screening.

2.10. Magnetic resonance imaging (MRI)

Imaging of tumor growth in GBM-tumor bearing mice was performed *via* MRI using a 7.0 T Bruker BioSpec 70/20 USR magnet with a murine head-coil. Mice were anesthetized with 3% isofluorane under O_2/N_2 supply while respiration was monitored. T2-w images were generated with a repetition time (TR) = 3750 ms, echo time (TE) = 44 ms and slice thickness = 0.5 mm. FOV = 192 cm × 192 cm. Matrix = 128 × 128. 31 image slices were acquired.

2.11. In vivo tumor implantation

G30-LRP neurospheres were grown to 70% confluency and tested for mycoplasma contamination. Then, neurospheres were dissociated with StemPro Accutase (Thermo Fisher Scientific) and single-cells counted. 50,000 cells in 2 μL of DPBS were injected *via* intra-cranial injection into the striatum of 8-week-old athymic nude female mice. Tumors were left to grow for 9 days and visualized *via* T2w-MRI for tumor growth confirmation.

2.12. Immunofluorescence staining of brain/tumor sections

Brain and tumor tissues were collected and placed in 10% formalin under constant rocking at 4 °C for ~48 h. Next, tissue was transferred to 30% sucrose (Sigma-Aldrich), 0.01% sodium azide (Sigma-Aldrich) and stored in the cold room under constant rocking for at least 24 h. Tissue was cryo-sectioned at 30 μm thickness. For DNA damage staining, tissue slides were incubated with rabbit or mouse anti-phospho-ser139 histone γH2AX antibody (Cell Signaling Technologies) at a dilution of 1:100. Cleaved-caspase 3 staining was performed in tissue slides with incubation of a rabbit anti-cleaved-caspase 3 (Cell Signaling Technologies) antibody at a dilution of 1:100. For astrocyte staining, tissue slides were incubated with mouse anti-GFAP (Cell Signaling Technologies) at a dilution of 1:300. Endothelial cells were stained with goat anti-CD31 (Abcam) at a dilution of 1:100. Neurons were stained with rabbit NeuN (Cell Signaling Technologies) at a dilution of 1:300. Next, slides were incubated appropriately with either goat anti-rabbit or anti-mouse antibody conjugated with Alexa Fluor 647 (Jackson Laboratory) at a dilution of 1:500, donkey anti-mouse, anti-rabbit or anti-goat antibody conjugated with Alexa Fluor 488 (Jackson Laboratory) and 1:1000 of Hoechst 33342 (Thermo Fisher Scientific) for nuclear staining. Slides were visualized *via* confocal microscopy.

2.13. Toxicity and maximum tolerated dose (MTD) studies

For pilot dose-tolerability studies, nude naïve female mice were injected *via* the tail-vein with either cisplatin at 5 mg/kg, Pt(IV)-M13 at 1.5 mg/kg, or Pt(IV)-M13 at 5 mg/kg. Dose regimes followed a bi-weekly injection. Mice were weighed every 2 days and symptomatology assessed using a clinical score: 0 = No symptoms, 1 = slightly visible, 2 = visible, 3 = very visible/damage, 4 = severe-fatal. Studies were stopped after detecting a score of 3 in any of the groups. MTD studies involved dose escalation of Pt(IV) and Pt(IV)-M13 treatment arms ranging from 5 mg/kg to 30 mg/kg.

2.14. Survival studies

For the first pilot survival study, G30-LRP tumors were implanted as described above. After 9 days post-tumor implantation, T2w MRI was performed for tumor growth confirmation. At day 10, a bi-weekly regime was initiated with 5 mg/kg of cisplatin or Pt(IV)-M13. Endpoint was reached when animal body weight was reduced by 20% and/or their body condition score was diminished. For the second survival study, the protocol was followed as above but including treatment arms of 15 mg/kg Pt(IV) or 15 mg/kg Pt(IV)-M13.

2.15. Statistical analysis

All quantifiable raw data were captured in Microsoft® Excel and transferred to GraphPad Prism v.9.3.0 for statistical analysis and graph plotting. Two-way ANOVA Šídák's multiple comparison test or Tukey's multiple comparison tests were performed as described in figure legends. Efficacy studies were analyzed using the Log-rank (Mantel-Cox) test. *p-value<0.05, **p-value<0.01, ***p-value<0.001, ****p-value<0.0001.

3. Results

3.1. Pt(IV)-M13 shows potent GBM cell killing in vitro

We previously described the synthesis and preliminary characterization of Pt(IV)-M13, a brain penetrant peptide-drug conjugate comprising M13, a perfluoroaryl stapled variant of the CPP TP10, and a Pt(IV) prodrug *cis*,*cis*,*trans*-[$Pt(NH_3)_2Cl_2(OH)_2$] (Fig. 1a) [23]. After cell entry, the Pt(IV) prodrug complex is designed to undergo reduction and release cisplatin [24,35,36]. We confirmed the release of Pt(IV) from the M13 peptide by reduction with ascorbic acid (Fig. S1a,b), [37] which showed succination of M13 peptide after Pt(IV) release. To assess the cytotoxicity of Pt(IV)-M13, we examined its effects on a panel of GBM cell lines grown as neurospheres and compared them to the non-conjugated Pt(IV) and cisplatin. Pt(IV)-M13 efficiently decreased cell viability in all the tested GBM cell lines as measured by the CellTiter-Glo 3D luminescent cell viability assay (Fig. 1b), with absolute IC_{50} values shown in Table S1. Pt(IV)-M13 demonstrated significantly more cytotoxicity than non-conjugated Pt(IV) in the tested cell lines G9-pCDH (0.59 fold-change IC_{50}, $p < 0.0001$), G30-LRP (0.69 fold-change IC_{50}, $p < 0.05$), G34-pCDH (0.19 fold-change IC_{50}, $p < 0.0001$) and GBM-X6 (0.71 fold-change IC_{50}, $p < 0.0001$) (Fig. 1c). Compared with cisplatin, the IC_{50} values of Pt(IV)-M13 were similar in G34-pCDH (1.33 fold-change IC_{50}, $p = 0.07$) and BT286 (4 fold-change IC_{50}, $p = 0.71$) cells, but significantly higher in G9-pCDH (2.5 fold-change IC_{50}, $p < 0.0001$) and G30-LRP (4.9 fold-change IC_{50}, $p < 0.001$) cell lines (Fig. 1c). Moreover, Pt(IV)-M13 shows higher toxicity than non-conjugated Pt(IV) prodrug and single M13 peptide, especially in the lower molar concentration ranges (Fig. S2a-d).

These data were corroborated in cell proliferation assays to evaluate GBM neurosphere growth. Quantification of neurosphere size confirmed Pt(IV)-M13 to be significantly superior to Pt(IV) in G9-pCDH and in G34-pCDH cells over a range of concentrations (Fig. 1d). Pt(IV)-M13 reduced the growth of G9-pCDH neurospheres but not to the extent of cisplatin (Fig. 1e). In the case of G34-pCDH cells, the inhibition of neurosphere growth by Pt(IV)-M13 remained superior to Pt(IV) at higher doses ($p < 0.05$) but also similar to cisplatin treatment (Fig. 1f). To investigate the higher toxicity exerted by Pt(IV)-M13 relative to the Pt(IV) prodrug, we performed platinum detection in GBM neurospheres *via* ICP-MS. Platinum levels were considerably higher in Pt(IV)-M13-treated cells than those with cisplatin or Pt(IV) prodrug (Figs. S4a,b), suggesting a higher platinum delivery capacity in the peptide complex than non-conjugated Pt(IV), which could explain the increased toxicity caused by the Pt(IV)-M13 complex relative to Pt(IV) alone.

Overall, Pt(IV) treatment showed the weakest effect on neurosphere growth, supporting the idea that conjugation of the Pt(IV) prodrug to the M13 peptide increased its cytotoxicity and suppression of neurosphere growth against GBM cell lines.

3.2. Pt(IV)-M13 is taken up efficiently into BBB spheroids in an energy-dependent manner

Previously, we developed a three-dimensional spheroid model of the BBB that retains biological features of an intact BBB [33] and can be used to qualitatively assess drug and peptide BBB-penetration *in vitro* [38]. BBB spheroids were incubated with either Pt(IV)-M13, Pt(IV) prodrug or cisplatin for 3 h and platinum levels were quantified by ICP-MS (Fig. 2a). BBB spheroids treated with Pt(IV)-M13 showed a dose-dependent uptake of platinum (Fig. 2b) (mean 16.4 ng/mL at 1 μM and 24.5 ng/mL at 5 μM). Conversely, BBB spheroids showed minimal platinum uptake when treated with either cisplatin (mean 0.2 ng/mL at 1 μM and 0.4 ng/mL at 5 μM) or the Pt(IV) prodrug alone (mean 0.2 ng/mL at 1 μM and 0.7 ng/mL at 5 μM), in accordance with their known lack of BBB penetration [39]. These data show that the conjugation of the Pt(IV) prodrug with the M13 peptide can increase platinum uptake in the BBB spheroid model.

To investigate the mechanism of Pt(IV)-M13 uptake, we incubated BBB spheroids with 1 μM Pt(IV)-M13 or cisplatin at 4 °C or 37 °C (Fig. 2a). Spheroids treated with Pt(IV)-M13 showed a significant ~4-fold decrease in platinum content at 4 °C relative to 37 °C, suggesting that an active transport mechanism is responsible for the platinum uptake when using Pt(IV)-M13 (Fig. 2b). Cisplatin internalization was also decreased at 4 °C (by ~3-fold), suggesting that energy-dependent uptake mechanisms are similarly involved.

To address whether the increased platinum concentration is due to specific Pt(IV)-M13 internalization, and not to compromised BBB spheroid barrier integrity as a result of non-specific toxicity, we incubated our platinum compounds with BBB spheroids as above and performed a TRITC-labelled dextran (155 kDa) permeability assay [33,34]. Mean fluorescence intensity quantification at 85 μm depth into the spheroid core did not show increased dextran internalization upon Pt(IV)-M13 or Pt(IV) incubation when compared with controls (Fig. 2d and e), indicating that the Pt(IV) prodrug compounds do not alter BBB spheroid integrity. Cisplatin addition led to higher fluorescence intensity than the control (p-value = 0.04), which may be attributed to possible drug-related toxicity in the *in vitro* model.

3.3. Biodistribution, pharmacokinetics and uptake of Pt(IV)-M13 in GBM tumors in vivo

To understand the BBB-penetrating properties and biodistribution of platinum in GBM tumor-bearing mice, we measured platinum levels following tail-vein injection with the various compounds by ICP-MS according to the scheme outlined in Fig. 3a. We initially collected organs 5 h after administration of 1.5 mg/kg of either Pt(IV)-M13 or cisplatin as described in our previous studies in healthy mice [23]. The cohort treated with Pt(IV)-M13 showed ~7-fold increase in platinum uptake relative to cisplatin in healthy brain (p-value <0.0001) and ~ 8-fold in tumor tissue (p-value <0.0001) (Fig. 3b and c), demonstrating that M13 conjugation to a Pt(IV) prodrug enhances uptake across the BBB and allows elevated platinum concentrations in the brain and tumor. These observations recapitulate our previous work in healthy mouse brain, which showed ~15-fold increase of platinum in the brain [23]. Differences between the uptake levels of Pt(IV)-M13 and cisplatin groups were also observed in spleen (mean 2-fold difference, p-value = 0.027) and heart (mean 0.6-fold difference, p-value = 0.027). No significant differences were seen in the lungs and kidneys, which are known to be the main sites for platinum drug accumulation [40]. The liver showed a 4-fold increased accumulation of Pt(IV)-M13 over cisplatin, albeit not statistically significant (p-value = 0.08).

To explore the pharmacokinetics of platinum accumulation in healthy brain and tumor tissues, we administered 1.5 mg/kg of Pt(IV)-M13 conjugate to G30-LRP tumor-bearing nude mice and collected brain and tumor tissues over time for ICP-MS analysis (Fig. 3d). Platinum accumulation peaked at 5 h after Pt(IV)-M13 administration in healthy brain and tissue. Subsequent timepoints showed a decrease in platinum levels at 8 h that remained consistent for up to 24 h, but these differences were not significant compared with the 5 h platinum peak levels.

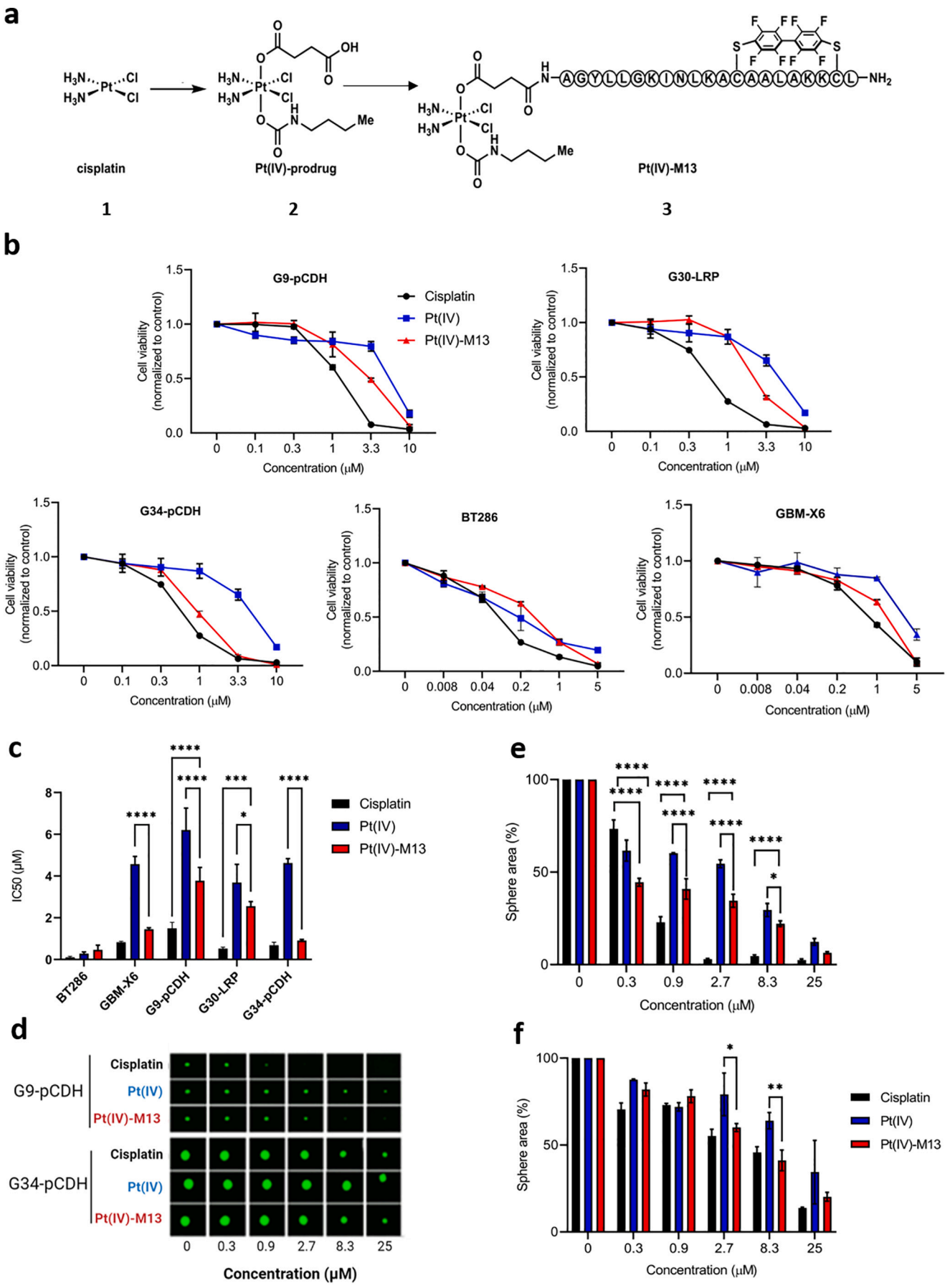

(caption on next page)

Fig. 1. The Pt(IV)-M13 peptide-drug conjugate exerts cytotoxic effects *in vitro*. a) Chemical structures of the tested platinum compounds: 1) cisplatin, 2) Pt(IV) prodrug and 3) the Pt(IV)-M13 peptide conjugate. b) Cell viability of GBM cell lines treated in the presence of cisplatin, Pt(IV) and Pt(IV)-M13 for 4 days. Concentrations shown in μM. Results are shown as relative values to non-treated controls. Cell viability was measured using the CellTiter-Glo 3D assay. Each point represents mean and standard deviation at the indicated concentration. c) Bar chart of IC_{50} values for each cell type upon cisplatin, Pt(IV) prodrug and Pt(IV)-M13 treatment. Mean and standard deviation, $n = 3$. d) Growth-in-low attachment (GILA) assay for assessing G9-pCDH and G34-pCDH neurosphere formation in the presence of Pt(IV)-M13, Pt(IV) prodrug or cisplatin. GFP channel (488 nm) was used for image acquisition at day 4 after compound addition. e) and f) Percentage of sphere area quantification relative to non-treated control from assays in d) G9-pCDH cells and G34-pCDH cells. All experimental data are presented in triplicates. Sidak's multiple comparison test * p-value<0.05, ** p-value<0.01, *** p-value<0.001, **** p-value<0.0001.

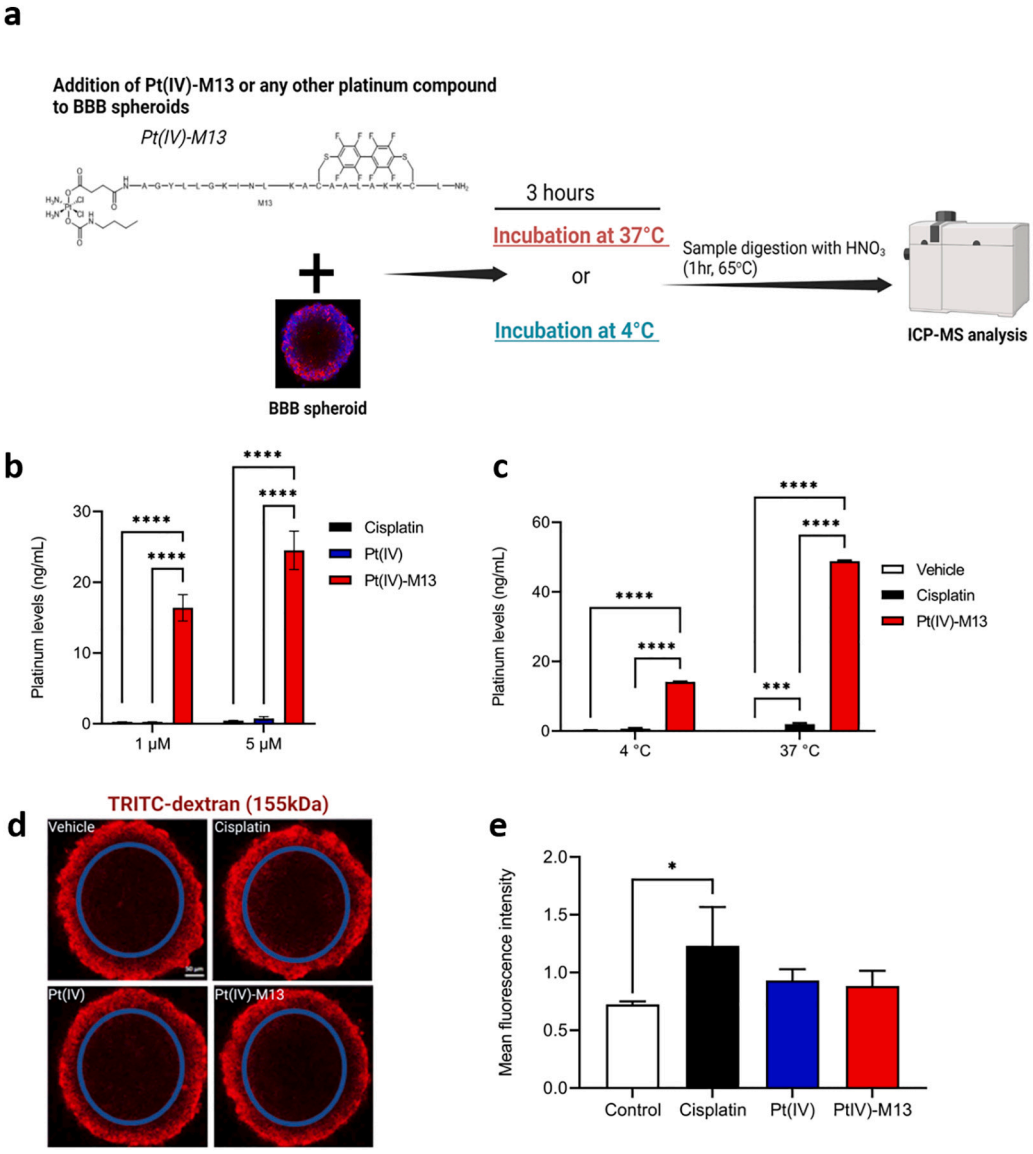

Fig. 2. Pt(IV)-M13 is internalized into BBB spheroids in an energy-dependent manner. a) Experimental workflow for the BBB spheroid incubation with platinum compounds (Pt(IV)-M13, Pt(IV) prodrug or cisplatin) for ICP-MS analysis for platinum quantification and incubation at 37 °C or 4 °C for uptake mechanism studies. Figures were generated in Biorender.com. b) Platinum (^{195}Pt) quantification *via* ICP-MS. Each compound was added at the indicated concentration for 3 h into BBB spheroids. c) Intracellular platinum content quantification from BBB spheroids treated with either 1 μM of Pt(IV)-M13 or cisplatin and incubated for 3 h at the indicated temperatures. Mean and SD are shown from triplicates. d) Dextran permeability in BBB spheroids. TRITC-labelled dextran (155 kDa, red) was co-incubated for 3 h with BBB spheroids treated with each compound and visualized under confocal microscopy at 85 μm depth (within blue circle). Image is a representative picture of a triplicate of photos. Scale bar = 50 μm. e) Mean fluorescent quantification of TRITC-dextran permeability shown within the blue circle of d). For b), c) and e) mean and SD are shown from triplicates, two-way ANOVA test. Significance at *$p < 0.05$, ***$p < 0.001$, ****$p < 0.0001$. (For interpretation of the references to colour in this figure legend, the reader is referred to the web version of this article.)

3.4. Dosage regimen and efficacy studies of Pt(IV)-M13 reveal DNA-damage effects on GBM tumors

Previous studies have reported that the maximum tolerated dose (MTD) for cisplatin in mice is approximately 5 mg/kg [41,42]. Additionally, pre-clinical studies report that bi-weekly administration of cisplatin at MTD doses improved survival in peripheral tumor-bearing mice [41]. We thus used the cisplatin MTD of 5 mg/kg as a constant dosing schedule reference for investigating the pharmacology of the Pt (IV)-M13 conjugate. Naïve nude mice were injected with either Pt(IV)-

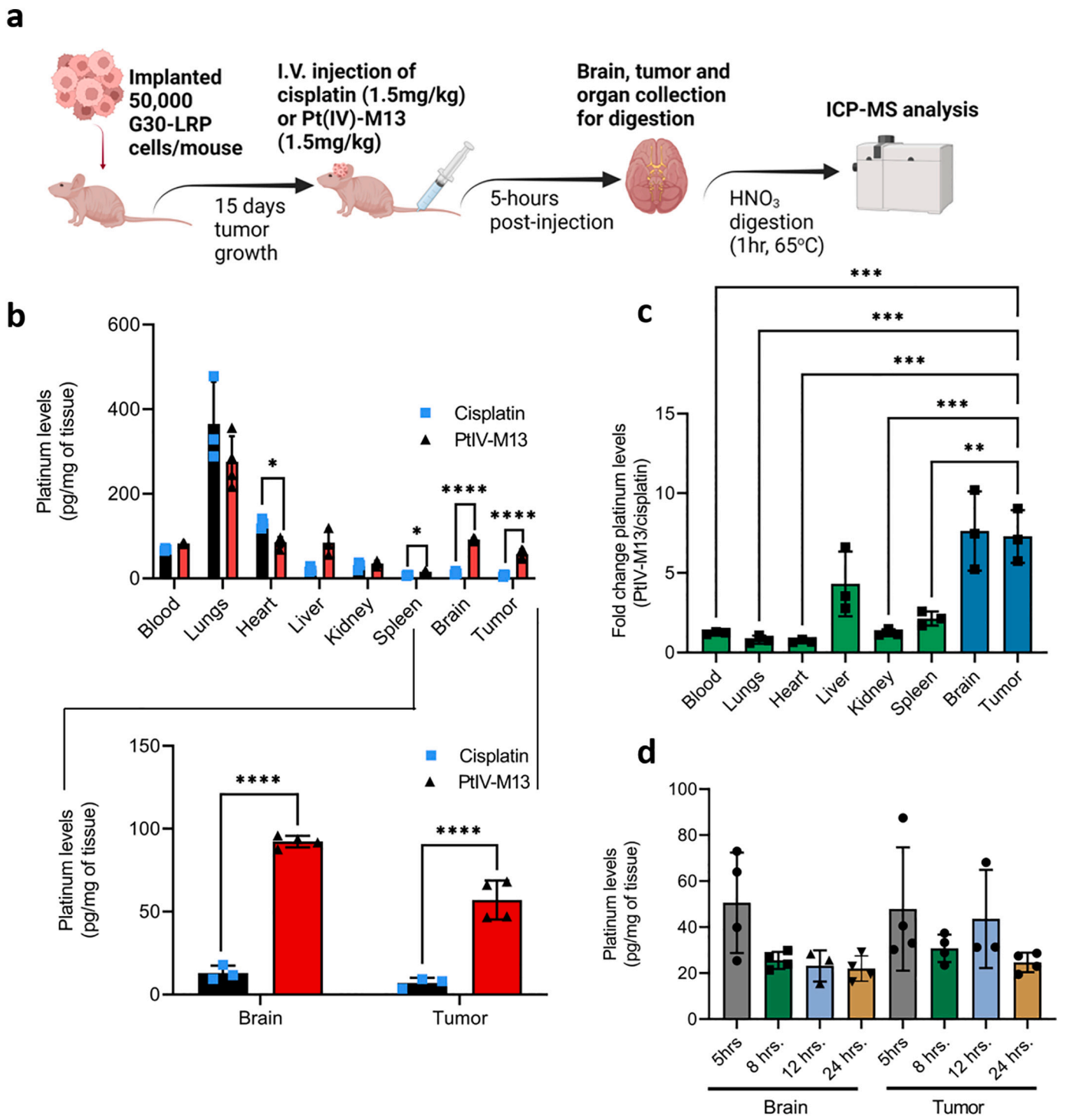

Fig. 3. Platinum biodistribution and uptake kinetics after Pt(IV)-M13 administration in a GBM xenograft murine model. a) Scheme of experimental approach for G30-LRP tumor implantation in naïve nude mice, tail-vein administration of platinum compounds and organ collection for platinum quantification by ICP-MS (^{195}Pt). b) Platinum levels in different organs after 5 h of treatment with 1.5 mg/kg of either Pt(IV)-M13 or cisplatin. Brain and tumor levels are shown separately to highlight platinum uptake by Pt(IV)-M13 in brain and tumor tissue above cisplatin; $n = 3$–4 mice/group. c) Fold-change of Pt(IV)-M13/cisplatin from experiment shown in b). Mean and standard deviation are shown, $n = 3$. d) Platinum distribution kinetics in brain and GBM tumor after administration of 1.5 mg/kg of Pt(IV)-M13 *via* tail-vein. Mean and standard deviation are shown, $n = 4$. Statistical analysis for b) and d) involved two-way ANOVA test. $^{*}p < 0.05$, $^{****}p < 0.0001$. Statistical analysis for c) involved one-way ANOVA test, $^{**}p < 0.005$, $^{***}p < 0.0005$. d) did not show any significant differences among groups.

M13 or cisplatin *via* tail-vein and body weight-change was assessed as shown in Fig. 4a. During the first 14 days of treatment, we did not identify any significant differences in weight and clinical score between groups. Pt(IV)-M13 administration did not lead to any significant weight differences at any time point at 1.5 mg/kg or 5 mg/kg, suggesting that these doses are safe for use in nude mice and feasible for preliminary survival studies. Conversely, we detected a trend of weight decrease in the cisplatin group from day 16 to day 20, albeit not significant, accompanied by grade 2 average clinical scores, as can be expected from a MTD dosing regimen (Fig. 4b).

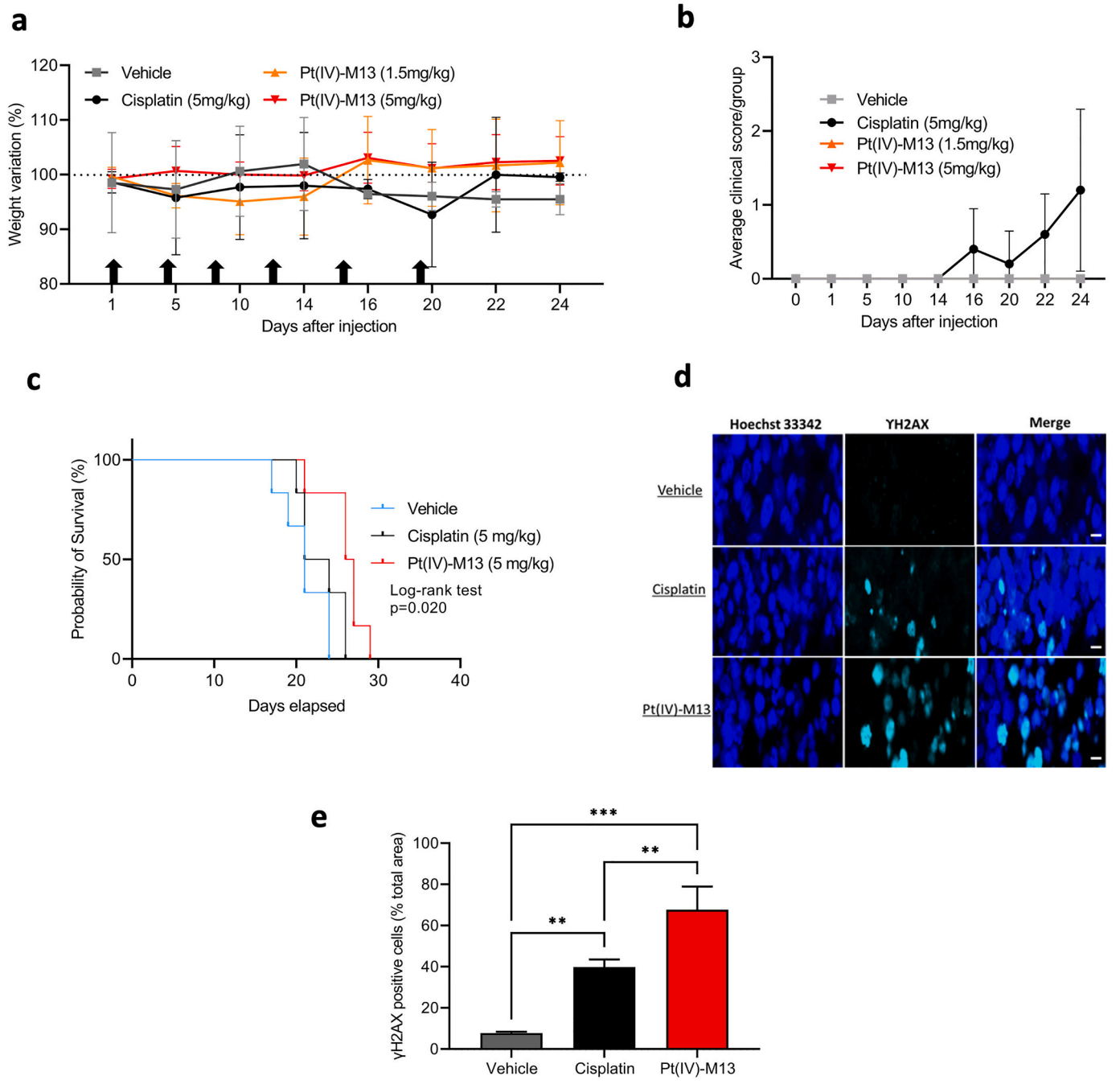

Fig. 4. Dose-regime and efficacy studies of Pt(IV)-M13 reveal DNA-damage effects on GBM tumors. a) Percentage of weight variation of naïve nude mice administered after platinum compound tail-vein injection at the indicated concentrations. Black arrows indicate days of injection (d1, d4, d9, d13, d17, d19). Mean and standard deviation are shown, $n = 5$ animals per group. b) Average clinical score from study shown in a). Mice were monitored every 2 days for symptomatic changes. Symptoms were classified from no symptoms (0), visible (2), to fatal (4). Eye redness, eye twitching and weight loss were the most visible effects. c) Efficacy study of Pt(IV)-M13 (5 mg/kg, 0.3 mM) compared to cisplatin MTD (5 mg/kg, 3 mM). d) Immunostaining of ϒH2AX (Ser139) using anti-rabbit Alexa Fluor 647, and nuclei with Hoechst 33342. Representative image of independent tissue triplicates from the efficacy study c). Scale bar, 10 μm. e) Area percentage of positive cells with ϒH2AX foci within the tumor core from study in d). Statistical significance for c) using log-rank test, $^{*}p = 0.020$. Median survival for each group is shown. For e), mean and standard deviation are shown, $n = 3$. Two-way ANOVA test $^{**}p < 0.005$, $^{***}p = 0.0004$.

Next, we tested the effects of Pt(IV)-M13 at 5 mg/kg on GBM growth *in vivo*. We implanted G30-LRP cells in naïve nude mice. On day 10, we started a bi-weekly regime of platinum compound administration *via* tail-vein injection (Fig. 4c). The Pt(IV)-M13 treatment showed a significant survival advantage over control mice (median survival 26.5 days for Pt(IV)-M13 *vs* 21 days for control, log-rank *p*-value = 0.0056), and a statistically non-significant increase in survival over the cisplatin group (median survival 26.5 days for Pt(IV)-M13 *vs* 22.5 days for cisplatin, log-rank p-value = 0.45). Thus, Pt(IV)-M13 confers a survival advantage to tumor-bearing mice over controls and cisplatin treatments at equivalent mass dosing.

To assess the effects of Pt(IV)-M13 on tumors *in vivo*, we performed confocal immunofluorescence microscopy for the DNA damage marker γH2AX (Fig. 4d). Treatment with either Pt(IV)-M13 or cisplatin increased γH2AX levels, while the non-treated control remained negative, demonstrating that the Pt(IV)-M13 conjugate is biologically active

and leads to DNA damage *in vivo*. The Pt(IV)-M13 treated group also showed a significantly higher frequency of γH2AX positive-nuclei when compared to cisplatin (mean 67.7 foci for the group treated with Pt(IV)-M13 *vs.* 39.7 for the group treated with cisplatin, p-value = 0.0078) (Fig. 4e). *In vitro* assessment of DNA damage showed the Pt(IV) prodrug moiety of the conjugate is responsible for the γH2AX positive-nuclei, as the M13 peptide alone did not display observable DNA-damaging activity (Fig. S3). These data suggest that the elevated platinum levels in the context of Pt(IV)-M13 treatment leads to increased DNA damage in tumors, likely accounting for the increased survival observed.

3.5. Elevated doses of Pt(IV)-M13 are well tolerated in mice

To further improve the efficacy of Pt(IV)-M13, we investigated whether higher doses could be tolerated in healthy mice. Increasing doses of Pt(IV)-M13 or non-conjugated Pt(IV) prodrug were administered alongside a cisplatin group at MTD dose of 5 mg/kg *via* systemic injection (Fig. 5a). Treatment of Pt(IV)-M13 was well-tolerated up to 15 mg/kg, as no overt weight variations or clinical symptoms were observed. At the 30 mg/kg dose, mice began to show a small decrease in weight, albeit non-significant compared with other groups (Fig. 5b), as well as visible clinical symptoms, such as eye redness and myoclonia (Fig. 5c). These effects were comparable to cisplatin after 16 days of treatment and show that Pt(IV)-M13 is well-tolerated in mice at mass doses of up to 3-fold higher than the MTD of cisplatin (15 mg/kg Pt(IV)-M13 over 5 mg/kg cisplatin) and could be administered as such for efficacy studies. γH2AX staining in healthy brain regions of mice treated with 15 mg/kg Pt(IV)-M13 or MTD cisplatin showed that Pt(IV)-M13 does not provoke more DNA damage relative to cisplatin in astrocytes, endothelial cells or neurons (Fig. S5a-f), suggesting tolerability in the CNS compartment. Taken together, these studies indicate the significant reduction in cisplatin systemic toxicity conferred by conjugation of a Pt (IV) prodrug to a bioactive BBB-penetrating peptide.

3.6. Administration of Pt(IV)-M13 at elevated doses significantly extends survival of GBM-tumor bearing mice over cisplatin and Pt(IV) prodrug

To investigate the effects of Pt(IV)-M13 at its highest tolerated dose (15 mg/kg, twice weekly) on tumor growth in GBM-bearing animals we adopted the treatment schedule shown in Fig. 6a. No drug-related side-effects were observed and the Pt(IV)-M13 cohort showed a significant survival increase above all control groups (median survival 33 days, log-

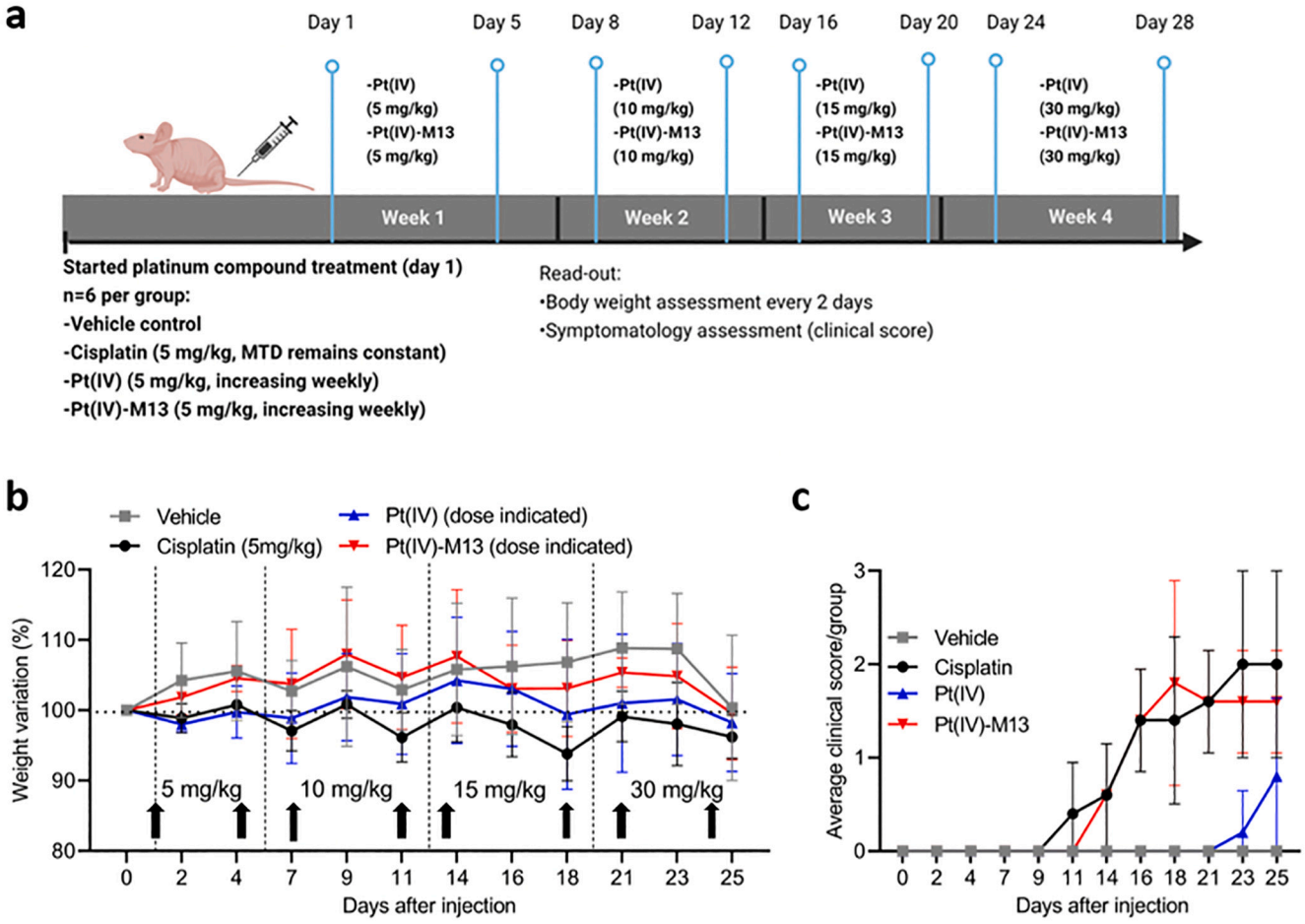

Fig. 5. Maximum tolerated dose studies (MTD) of the Pt(IV)-M13 peptide conjugate. a) Scheme of dose regime studies of Pt(IV)-M13 in nude naïve mice. Injection days are indicated along with dosages of the unconjugated Pt(IV) prodrug and Pt(IV)-M13 for each week. Figure was generated in Biorender.com. b) Percentage of weight variation upon platinum compound administration. Black arrows indicate day of administration and at the concentration shown for each week (week 1: d1 and d4, week 2: d7 and d11, week 3: d14 and d18, week 4: d21 and d24). Black dotted line represents 100% basal weight. Cisplatin remained constant at its MTD dose of 5 mg/kg ($n = 5$ mice per group). Mean and standard deviation are shown. c) Average clinical score per group from study in b). Mice were monitored every 2 days for symptomatology changes. Symptoms were classified in from no symptoms (0) to severe to fatal (4). Eye redness, eye twitching and weight loss (scores 2–3) were the most visible effects. The study was halted when the cisplatin and Pt(IV)-M13 groups started showing visible symptoms. Mean and standard deviation are shown, $n = 5$.

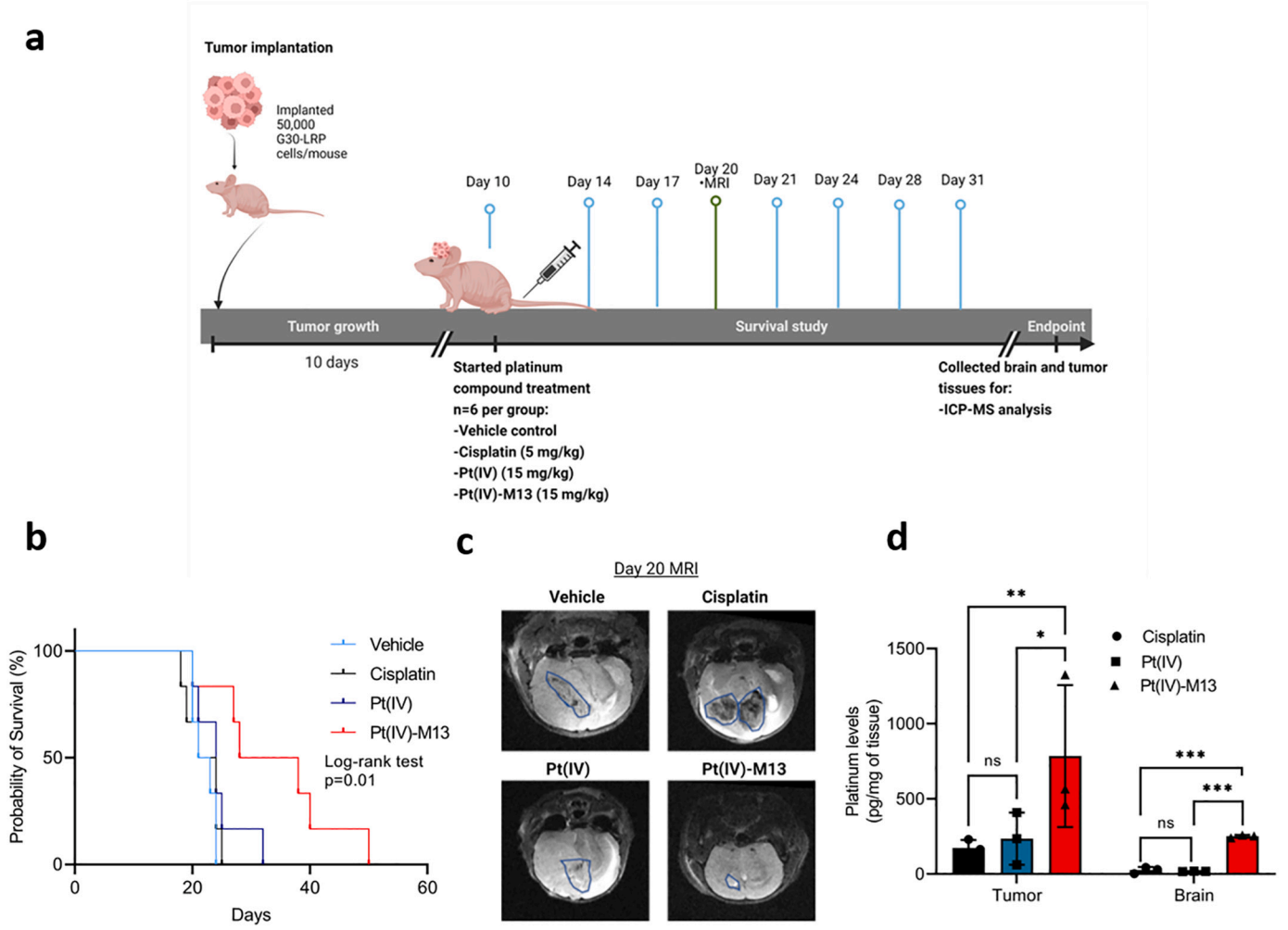

Fig. 6. High doses of Pt(IV)-M13 improve GBM tumor-bearing mice survival and increase platinum intra-tumoral and brain uptake. a) Scheme of G30-LRP tumor implantation in naïve nude mice and subsequent treatment with each platinum compound for efficacy studies and platinum level quantification. Figure was generated in Biorender.com. b) Kaplan-Meier curve of tumor-bearing mice. Compound administration started at day 10 using a bi-weekly regime. Doses of 5 mg/kg cisplatin (3 mM), 15 mg/kg Pt(IV) (5 mM) and 15 mg/kg Pt(IV)-M13 (0.9 mM). c) Representative T2w MRI of a single mouse of each treatment arm at day 20 post-tumor implantation. Blue contours indicate tumor location. d) ICP-MS quantification of platinum in tumor and healthy brain tissues from efficacy study b). For b) median survival is shown, $n = 6$ mice per group, using log-rank test, $p = 0.01$. For c) and d), statistical significance was shown as mean and standard deviation, $n = 3$. Two-way ANOVA test, $*p < 0.05$, $**p = 0.0035$, $***p < 0.0001$. (For interpretation of the references to colour in this figure legend, the reader is referred to the web version of this article.)

rank p-value = 0.01) (Fig. 6b). Together with data shown in Fig. 4, this outcome suggests that increasing the dosage of Pt(IV)-M13 leads to improved efficacy in the G30-LRP xenograft model. On the other hand, cisplatin (median survival 22.5 days, log-rank = 0.62) and the Pt(IV) prodrug (median survival 24 days, log-rank p-value = 0.14) treated groups showed no significant survival advantage over the non-treated control group (median survival 22 days, log-rank p-value = 0.62).

We performed MRI analysis of tumor growth during treatment (20 days after tumor implantation) to assess tumor growth behavior between groups when mice started to meet defined endpoints in the control arm (Fig. 6c). This showed that the Pt(IV)-M13 treated mice presented a smaller tumor size when compared to other cohorts, in agreement with the improved efficacy shown by Pt(IV)-M13. Platinum quantification in healthy brain and tumor tissue from end-point mice revealed higher platinum levels in the Pt(IV)-M13 treatment group when compared to cisplatin and Pt(IV) prodrug groups (Fig. 6d). Cellular death due to Pt(IV)-M13 was mainly observed in tumor but not in healthy brain when end-point tumor and brain tissues were stained for cleaved caspase-3 (Fig. S6). Thus, we have shown for the first time that the conjugation of a cisplatin prodrug (Pt(IV)) to a macrocyclic cell-penetrating peptide (M13) leads to efficacious dosing in mice at three times higher MTD than cisplatin alone, conferring significant survival advantages in murine GBM models.

4. Discussion

The BBB represents a daunting challenge in the treatment of diseases of the CNS. The BBB prevents the accumulation of the great majority of anti-neoplastic drugs, which represents an obstacle in the effective treatment of brain cancer. To address this problem, we have leveraged the biological membrane-crossing properties of CPPs to impart BBB penetration abilities to a conjugated cisplatin Pt(IV) prodrug. Our approach leverages the cell-penetrating properties of the TP10 peptide, which were further enhanced by incorporation of a perfluoroaryl macrocycle to create M13 [43]. The resulting Pt(IV)-M13 conjugate represents the first agent of its class designed for brain cancer therapy. The evaluation of symptomatology presented in mice treated with the Pt(IV)-M13 conjugate revealed that the peptide is well tolerated at doses three times higher than the cisplatin MTD. Pt(IV)-M13 treatment increased intra-tumoral platinum accumulation and extended the survival of brain

tumor-bearing mice at these doses, while showing DNA-damaging effects by γH2AX immuno-staining. Together, these data provide the first evidence supporting the use of macrocyclic CPPs as vehicles to improve the delivery of chemotherapeutics to GBM.

In the context of GBM cell-killing activity, Pt(IV)-M13 showed greater potency than the Pt(IV) prodrug alone, supporting that its conjugation with the M13 peptide is beneficial toward improving efficacy, potentially due to enhanced cell penetration imparted by the M13 moiety. This could be explained due to the increased platinum content delivered *via* the Pt(IV)-M13 complex rather than the Pt(IV) prodrug alone (Fig. S3 a and b). Nonetheless, Pt(IV)-M13 overall presented slightly reduced cytotoxicity than cisplatin (Fig. 1b). Our data showed similar IC_{50} values of Pt(IV)-M13 and cisplatin in G34-pCDH and GBM-X6 cells, but not in G9-pCDH and G30-LRP cells. Platinum resistance is a common event in cancer patients, and several mechanisms are known to be responsible for driving resistance against platinum drugs, such as increased DNA-damage repair mechanisms, low influx of platinum or secretion that reduce intra-cellular accumulation [44,45]. Additionally, Pt(IV) prodrugs can be less potent than their Pt(II) forms due to additional biochemical processes required to achieve activation, which also diminishes systemic toxicity outcomes [46]. Regarding this notion, factors such as cell line-specific intracellular reducing environments, thiol-dependent platinum inactivation and differential platinum-conjugate uptake between cell lines can be relevant elements in determining Pt(IV) to Pt(II) conversion yield and its cytotoxicity [47,48]. In the *in vivo* setting, intracellular reduction of Pt(IV) prodrugs is mainly driven by tissue-specific levels of ascorbate [37] and glutathione (GSH), or other reductants, such as metallothionein, that can also play a role in the Pt(IV) to Pt(II) conversion [48]. Our work highlighted the capacity of ascorbate to release the Pt(IV) moiety from the M13 peptide. Indeed, aqueous extracts from a range of cancer cell lines from different tissues showed distinctive reduction yields of the same Pt(IV) prodrug, which was driven by cell intrinsic reductants of diverse nature [49]. Other studies showed that differential intracellular GSH levels influence the activation yield of satraplatin, another Pt(IV) prodrug, which resolves in differential cytotoxicity among cell types [50]. Altogether, these elements could be involved in the differential sensitivity of our GBM cell lines to Pt(IV)-M13 treatment.

On the other hand, Pt(IV) prodrugs are mainly designed to minimize cytotoxic effects in healthy tissue, since non-cancerous cells do not present reductive capacities (higher GSH levels) relative to the tumor environment [51]. Previously we have shown that our Pt(IV) prodrug does not exert cytotoxic activities in HCMEC/D3 endothelial cells and primary astrocytes *in vitro*; moreover, liver tissue from nude mice treated with Pt(IV)-M13 did not show increased DNA damage when compared to cisplatin [23]. In parallel, ongoing research on novel palliative care strategies is taking place to reduce platinum-derived toxicity, and which could be applicable to our Pt(IV)-M13 complex. For instance, silk-polyethylene glycol hydrogels loaded with dexamethasone alleviated cisplatin-induced ototoxicity in guinea pig and murine models [52]. Combinatorial therapies also enable reduction of toxic chemotherapy dosing, while enhancing clinical outcomes. For example, curcumin in combination with cisplatin chemotherapy attenuates platinum-induced off-target effects by boosting cisplatin anti-cancer cytotoxicity, which in turn allows for reduced doses of cisplatin [53]. We currently are investigating the use of combination strategies with our Pt(IV)-M13 prodrug for potentiating its therapeutic effects and to reduce possible off-target toxicities.

Platinum uptake studies *in vitro* using our BBB spheroid model [33,43] showed enhanced platinum accumulation upon Pt(IV)-M13 treatment compared with cisplatin and Pt(IV) prodrug controls (Fig. 2b), suggesting that the Pt(IV) moiety upon conjugation to the M13 peptide gains BBB-penetrating abilities. When BBB spheroids were incubated with Pt(IV)-M13 at 4 °C (Fig. 2c), platinum delivery was decreased, suggesting an energy-dependent mechanism such as endocytosis [54] is responsible for cellular internalization. Intriguingly, TP10, the non-stapled version of M13, has been suggested to internalize *via* non-endocytic mechanisms, since endocytosis inhibitors do not block its cellular uptake, although these studies did not interrogate TP10 uptake at low temperature [55]. Still, the addition of the macrocyclic moiety, and the Pt(IV) conjugation, might render other mechanisms of cellular uptake available to the Pt(IV)-M13 conjugate. Moreover, decreased cisplatin uptake was also observed at low temperature. This observation correlates with other research supporting the notion that cisplatin intracellular uptake is temperature-dependent [56].

Other energy-dependent mechanisms, such as receptor-mediated BBB-penetration, have been leveraged in combination with CPPs. Docetaxel (DTX)-loaded nanomicelles hybridized with Angiopep-2 increased intra-tumoral localization of docetaxel in a U87MG murine model. ANG20-DTX peptides accumulated in tumor but intra-tumoral penetration and retention times were increased when a TAT CPP moiety was conjugated to the complex [57]. Production of targeted CPPs accumulate the peptide complexes in the brain tumor, rather than in peripheral tissue, increasing drug uptake and efficacy. Other receptor-mediated BBB-targeting studies involve transferrin receptor-mediated delivery of siEGFR in glioblastoma [58,59] and LRP1-mediated delivery of doxorubicin in a 231-BR brain metastasis model [59], both showing promising drug uptake in tumor and pre-clinical efficacy. Macrocyclization of CPPs increase their stability and penetration capacities, as seen with our M13 peptide over the TP10 backbone. Future considerations for our Pt(IV)-M13 complex involve conjugation with targeting moieties to ensure accumulation in the tumor and augment clinical outcomes.

Detection of clinically relevant drug concentrations in brain tissue is important for GBM drug development. ICP-MS enables the precise quantification of metal contents at trace levels, being amenable to analysis of elements such as those contained in platinum and osmium [60] complexes, and further providing information about their biodistribution [61,62]. Indeed, other groups have confirmed the value of ICP-MS tools to assess trace-metal concentrations in tissue [63–66] and intratumorally in GBM [67,68] facilitating understanding of drug biodistribution, accumulation, and processing. In this regard, our findings suggested considerable platinum levels accumulate in healthy brain regions and in tumor tissue after 15 days of tumor growth (Figs. 3b) and in survival studies (Fig. 6d), showing that platinum-M13 conjugates penetrate the BBB and blood-tumor barrier regions. Future work will focus on testing Pt(IV)-M13 and other platinum-conjugated CPPs in additional GBM models, including recurrent GBM, metastatic brain cancer, and pediatric models.

Platinum distribution after Pt(IV)-M13 injection was similar to cisplatin in other tissues such as lungs, kidney and liver, but different in heart and spleen (Fig. 3b and c). It is known that platinum encapsulation or conjugation to a carrier changes systemic fate and biodistribution [69–71]. Nonetheless, platinum localizes considerably in peripheral organs, regardless of the carrier, reducing effective concentrations in tumors. Development of tumor-targeted platinum conjugates should be considered if tumor specificity and additional accumulation is desired.

Our platinum accumulation kinetics studies in brain and GBM tumor tissue (Fig. 3d) showed peak concentration at 5 h after Pt(IV)-M13 administration, and then showed declined platinum levels to a constant concentration for up to 24 h. Indeed, cisplatin can be detected in peripheral organs from tumor-bearing mice, such as kidney and liver, for up to 7 days post administration [72]. Moreover, compared to kidney, delayed clearance rate of platinum from the brain into the blood has been reported as well [73]. Clinically, peripheral organ accumulation of platinum after cisplatin or oxaliplatin chemotherapy has been reported in patients [74], and was associated with its toxic effects, such as nephrotoxicity [75] and ototoxicity [76]. Our MTD studies of Pt(IV)-M13 showed that no significant toxicity was observed following administration at approximately 3-fold higher doses than the reported cisplatin MTD (Fig. 5b and c), supporting the potential of Pt(IV) prodrugs to increase the therapeutic window.

Our previous work showed higher DNA platination levels in GBM cells treated with Pt(IV)-M13 compared with cisplatin treatment [23]. In this study, staining of γH2AX, a hallmark of DNA damage, in brain-tumor sections from the G30-LRP xenograft GBM murine model revealed the capacity of Pt(IV)-M13 to cause DNA-damage in tissue (Fig. 4d and e), which suggests that the Pt(IV) moiety of the conjugate becomes functional upon cellular internalization. This correlated with increased survival of tumor-bearing mice treated with Pt(IV)-M13.

In summary, our work shows the relevance of developing platinum-conjugated macrocyclic peptides for GBM therapeutics. Further studies on neurotoxicology and biodistribution should be pursued to understand the effects of higher platinum concentrations reaching healthy brain tissue. In this regard, alternative development of targeted conjugates and drug combination strategies, by conjugating axially two or four (in case of oxaliplatin) anti-cancer bioactive ligands such as p53 re-activators [77,78], should also be considered to maximize platinum efficacy and minimize off-site toxicity [79].

5. Conclusion

Our work highlights the potential of perfluoroaryl macrocyclic-stapled CPPs as drug delivery vehicles across the BBB for brain tumor treatment. Using mass spectrometry, we detected and quantified platinum accumulation in peripheral organs and tumoral tissue as a result of Pt(IV)-M13 administration. We performed kinetic analysis of Pt(IV)-M13 uptake, as well as organ biodistribution and toxicity studies in murine models. Pt(IV)-M13 retains its intended function when internalized as elucidated by γH2AX-based detection of DNA damage, delayed tumor growth and increased survival of animals in a GBM xenograft model. The Pt(IV)-M13 represents a potential approach for systemic delivery of GBM chemotherapeutics to the brain, overcoming the challenges posed by the BBB that currently prevent most oncological treatments. Future work will focus on expanding the usage of Pt(IV)-M13 to other brain tumor models under different BBB contexts to broaden its applicability and delineate its translation into further pre-clinical stages.

Data availability

All data generated or analyzed during this study are available either in the main text or supplementary materials.

CRediT authorship contribution statement

J.L. Jimenez-Macias: Conceptualization, Methodology, Data curation, Formal analysis, Investigation, Writing – original draft, Visualization, Project administration. **Y.-C. Lee:** Conceptualization, Methodology, Resources, Writing – review & editing, Visualization. **E. Miller:** Investigation, Writing – review & editing, Visualization, Resources. **T. Finkelberg:** Investigation, Writing – review & editing. **M. Zdioruk:** Investigation, Writing – review & editing. **G. Berger:** Methodology, Writing – review & editing, Visualization, Resources. **C.E. Farquhar:** Writing – review & editing, Resources. **M.O. Nowicki:** Methodology, Writing – review & editing, Resources. **C.-F. Cho:** Methodology, Writing – review & editing, Resources. **B.I. Fedeles:** Methodology, Resources, Writing – review & editing. **A. Loas:** Conceptualization, Methodology, Validation, Writing – review & editing, Resources. **B.L. Pentelute:** Conceptualization, Validation, Investigation, Resources, Writing – review & editing, Supervision, Funding acquisition. **S.E. Lawler:** Conceptualization, Validation, Investigation, Resources, Writing – original draft, Writing – review & editing, Supervision, Funding acquisition.

Declaration of Competing Interest

B.L.P. is a co-founder and/or member of the scientific advisory board of several companies focusing on the development of protein and peptide therapeutics.

Acknowledgments

This work was supported by a grant from the National Cancer Institute (R01-CA237063) to B.L.P. and S.E.L. Y.-C.L. gratefully acknowledges support from a Deutsche Forschungsgemeinschaft postdoctoral fellowship (DFG, LE 4224/1-1). E.M. was supported by a postdoctoral fellowship from the Ludwig Center at MIT's Koch Institute for Integrative Cancer Research. C.C.-F. was supported by the Brigham Research Institute, Sperling Family Foundation, Harvard Stem Cell Institute and Department of Defense (DOD grant number W81XWH1910791). C.E.F. (4000057441) acknowledges the National Science Foundation Graduate Research Fellowship program (Grant No. 1122374) for research support. ICP-MS instrumentation was supported by core center grant P30-ES002109 from the National Institute of Environmental Health Sciences, National Institutes of Health. B.F. was supported by National Institutes of Health grants R01-CA080024, P42-ES027707 and P30-ES002109. M.O.N. was supported by National Cancer Institute Grant R50-CA243706-02.

Appendix A. Supplementary data

Supplementary data to this article can be found online at https://doi.org/10.1016/j.jconrel.2022.10.051.

References

[1] M.D. Sweeney, Z. Zhao, A. Montagne, A.R. Nelson, B. Zlokovic, v., Blood-brain barrier: from physiology to disease and Back, Physiol. Rev. 99 (1) (2018) 21–78, https://doi.org/10.1152/physrev.00050.2017.
[2] P.S. Steeg, The blood–tumour barrier in cancer biology and therapy, Nat. Rev. Clin. Oncol. 18 (2021) 694–714, https://doi.org/10.1038/s41571-021-00529-6.
[3] K.E. Warren, Beyond the blood: brain barrier: the importance of central nervous system (CNS) pharmacokinetics for the treatment of CNS tumors, including diffuse intrinsic pontine glioma, Front. Oncol. 8 (JUL) (2018) 1–11, https://doi.org/10.3389/fonc.2018.00239.
[4] J.P. Thakkar, T.A. Dolecek, C. Horbinski, et al., Epidemiologic and molecular prognostic review of glioblastoma, Cancer Epidemiol. Biomark. Prev. 23 (10) (2014) 1985–1996, https://doi.org/10.1158/1055-9965.EPI-14-0275.
[5] B.S. Karmur, J. Philteos, A. Abbasian, et al., Blood-brain barrier disruption in neuro-oncology: strategies, failures, and challenges to overcome, Front. Oncol. (2020) 10, https://doi.org/10.3389/fonc.2020.563840.
[6] H.C. Lawson, P. Sampath, E. Bohan, et al., Interstitial chemotherapy for malignant gliomas: the Johns Hopkins experience, J. Neuro-Oncol. 83 (1) (2007) 61–70, https://doi.org/10.1007/s11060-006-9303-1.
[7] X. Dong, Current strategies for brain drug delivery, Theranostics. 8 (6) (2018) 1481–1493, https://doi.org/10.7150/thno.21254.
[8] R.K. Oberoi, K.E. Parrish, T.T. Sio, R.K. Mittapalli, W.F. Elmquist, J.N. Sarkaria, Strategies to improve delivery of anticancer drugs across the blood-brain barrier to treat glioblastoma, Neuro-Oncology 18 (1) (2016) 27–36, https://doi.org/10.1093/neuonc/nov164.
[9] H. Luo, E.V. Shusta, Blood–brain barrier modulation to improve glioma drug delivery, Pharmaceutics 12 (11) (2020), https://doi.org/10.3390/pharmaceutics12111085.
[10] W.M. Pardridge, Molecular Trojan horses for blood–brain barrier drug delivery, Curr. Opin. Pharmacol. 6 (5) (2006) 494–500, https://doi.org/10.1016/j.coph.2006.06.001.
[11] D.S. Hersh, A.S. Wadajkar, N. Roberts, et al., Evolving drug delivery strategies to overcome the blood brain barrier, Curr. Pharm. Des. 22 (9) (2016) 1177–1193, https://doi.org/10.2174/1381612822666151221150733.
[12] C.X. Deng, Targeted drug delivery across the blood-brain barrier using ultrasound technique, Ther. Deliv. 1 (6) (2010) 819–848, https://doi.org/10.4155/tde.10.66.
[13] B. Yuan, Y. Zhao, S. Dong, et al., Cell-penetrating peptide-coated liposomes for drug delivery across the blood–brain barrier, Anticancer Res. 39 (1) (2019) 237–243, https://doi.org/10.21873/anticanres.13103.
[14] B.M. Cooper, J. Iegre, D.H. O'Donovan, M.O. Lwegård Halvarsson, D.R. Spring, Peptides as a platform for targeted therapeutics for cancer: peptide-drug conjugates (PDCs), Chem. Soc. Rev. 50 (2020) 1480–1494, https://doi.org/10.1039/d0cs00556h.
[15] G. Appiah Kubi, P.G. Dougherty, D. Pei, Designing cell-permeable macrocyclic peptides, in: Methods in Molecular Biology vol. 2001, Humana Press Inc., 2019, pp. 41–59, https://doi.org/10.1007/978-1-4939-9504-2_3.
[16] E. Koren, V.P. Torchilin, Cell-penetrating peptides: breaking through to the other side, Trends Mol. Med. 18 (7) (2012) 385–393, https://doi.org/10.1016/j.molmed.2012.04.012.

[17] H. Gao, S. Zhang, S. Cao, Z. Yang, Z. Pang, X. Jiang, Angiopep-2 and Activatable cell-penetrating peptide dual-functionalized nanoparticles for systemic glioma-targeting delivery, Mol. Pharm. 11 (8) (2014) 2755–2763, https://doi.org/10.1021/mp500113p.
[18] G. Mehdipour, M.N. Wintrasiri, S. Ghasemi, CPP-Based Bioactive Drug Delivery to Penetrate the Blood-Brain Barrier: A Potential Therapy for Glioblastoma Multiforme. Curr Drug Targets, Published online, 2022.
[19] M. Shi, Z. Jiang, Y. Xiao, et al., Stapling of short cell-penetrating peptides for enhanced tumor cell-and-tissue dual-penetration, Chem. Commun. 58 (14) (2022) 2299–2302, https://doi.org/10.1039/d1cc06595e.
[20] H. Ruan, X. Chen, C. Xie, et al., Stapled RGD peptide enables glioma-targeted drug delivery by overcoming multiple barriers, ACS Appl. Mater. Interfaces 9 (21) (2017) 17745–17756, https://doi.org/10.1021/acsami.7b03682.
[21] J.M. Wolfe, C.M. Fadzen, R.L. Holden, M. Yao, G.J. Hanson, B.L. Pentelute, Perfluoroaryl bicyclic cell-penetrating peptides for delivery of antisense oligonucleotides, Angew. Chem. Int. Ed. 57 (17) (2018) 4756–4759, https://doi.org/10.1002/anie.201801167.
[22] C.M. Fadzen, J.M. Wolfe, C.F. Cho, E.A. Chiocca, S.E. Lawler, B.L. Pentelute, Perfluoroarene–based peptide macrocycles to enhance penetration across the blood–brain barrier, J. Am. Chem. Soc. 139 (44) (2017) 15628–15631, https://doi.org/10.1021/jacs.7b09790.
[23] C.M. Fadzen, J.M. Wolfe, W. Zhou, et al., A platinum(IV) prodrug - perfluoroaryl macrocyclic peptide conjugate enhances platinum uptake in the brain, J. Med. Chem. 63 (13) (2020) 6741–6747, https://doi.org/10.1021/acs.jmedchem.0c00022.
[24] T.C. Johnstone, K. Suntharalingam, S.J. Lippard, The next generation of platinum drugs: targeted Pt(II) agents, nanoparticle delivery, and Pt(IV) prodrugs, Chem. Rev. 116 (5) (2016) 3436–3486, https://doi.org/10.1021/acs.chemrev.5b00597.
[25] A. Brown, S. Kumar, P.B. Tchounwou, Cisplatin-based chemotherapy of human cancers, Cancers (Basel) 11 (4) (2019).
[26] S. Jacobs, C.L. McCully, R.F. Murphy, J. Bacher, F.M. Balis, E. Fox, Extracellular fluid concentrations of cisplatin, carboplatin, and oxaliplatin in brain, muscle, and blood measured using microdialysis in nonhuman primates, Cancer Chemother. Pharmacol. 65 (5) (2010) 817–824, https://doi.org/10.1007/s00280-009-1085-7.
[27] T. Zhang, S. Cai, W.C. Forrest, E. Mohr, Q. Yang, M.L. Forrest, Development and validation of an inductively coupled plasma mass spectrometry (ICP-MS) method for quantitative analysis of platinum in plasma, urine, and tissues, Appl. Spectrosc. 70 (9) (2016) 1529–1536, https://doi.org/10.1177/0003702816662607.
[28] M. Vojtek, E. Pinto, S. Gonçalves-Monteiro, et al., Fast and reliable ICP-MS quantification of palladium and platinum-based drugs in animal pharmacokinetic and biodistribution studies, Anal. Methods 12 (39) (2020) 4806–4812, https://doi.org/10.1039/d0ay01328e.
[29] N. McDannold, Y. Zhang, J.G. Supko, et al., Acoustic feedback enables safe and reliable carboplatin delivery across the blood-brain barrier with a clinical focused ultrasound system and improves survival in a rat glioma model, Theranostics. 9 (21) (2019) 6284–6299, https://doi.org/10.7150/thno.35892.
[30] N.U. Barua, K. Hopkins, M. Woolley, et al., A novel implantable catheter system with transcutaneous port for intermittent convection-enhanced delivery of carboplatin for recurrent glioblastoma, Drug Deliv. 23 (1) (2016) 167–173, https://doi.org/10.3109/10717544.2014.908248.
[31] S. Raghavan, D.S. Baskin, M.A. Sharpe, MP-Pt(IV): a MAOB-sensitive mitochondrial-specific prodrug for treating glioblastoma, Mol. Cancer Ther. 19 (12) (2020) 2445–2453, https://doi.org/10.1158/1535-7163.MCT-20-0420.
[32] A. Dréan, N. Lemaire, G. Bouchoux, et al., Temporary blood–brain barrier disruption by low intensity pulsed ultrasound increases carboplatin delivery and efficacy in preclinical models of glioblastoma, J. Neuro-Oncol. 144 (1) (2019) 33–41, https://doi.org/10.1007/s11060-019-03204-0.
[33] C.F. Cho, J.M. Wolfe, C.M. Fadzen, et al., Blood-brain-barrier spheroids as an in vitro screening platform for brain-penetrating agents, Nat. Commun. 8 (2017) 1–14, https://doi.org/10.1038/ncomms15623.
[34] S. Bergmann, S.E. Lawler, Y. Qu, et al., Blood–brain-barrier organoids for investigating the permeability of CNS therapeutics, Nat. Protoc. 13 (12) (2018) 2827–2843, https://doi.org/10.1038/s41596-018-0066-x.
[35] X. Han, J. Sun, Y. Wang, Z. He, Recent advances in platinum (IV) complex-based delivery systems to improve platinum (II) anticancer therapy, Med. Res. Rev. 35 (6) (2015) 1268–1299, https://doi.org/10.1002/med.21360.
[36] S. Choi, C. Filotto, M. Bisanzo, et al., Reduction and Anticancer Activity of Platinum(IV) Complexes. https://pubs.acs.org/sharingguidelines, 1998.
[37] Y.R. Zheng, K. Suntharalingam, T.C. Johnstone, et al., Pt(IV) prodrugs designed to bind non-covalently to human serum albumin for drug delivery, J. Am. Chem. Soc. 136 (24) (2014) 8790–8798, https://doi.org/10.1021/ja5038269.
[38] C.M. Fadzen, J.M. Wolfe, C.F. Cho, E.A. Chiocca, S.E. Lawler, B.L. Pentelute, Perfluoroarene-based peptide macrocycles to enhance penetration across the blood-brain barrier, J. Am. Chem. Soc. 139 (44) (2017) 15628–15631, https://doi.org/10.1021/jacs.7b09790.
[39] S. Jacobs, C.L. McCully, R.F. Murphy, J. Bacher, F.M. Balis, E. Fox, Extracellular fluid concentrations of cisplatin, carboplatin, and oxaliplatin in brain, muscle, and blood measured using microdialysis in nonhuman primates, Cancer Chemother. Pharmacol. 65 (5) (2010) 817–824, https://doi.org/10.1007/s00280-009-1085-7.
[40] J. Uozumi, T. Ueda, T. Yasumasu, et al., Platinum accumulation in the kidney and liver following chemotherapy with cisplatin in humans, Z. Urol. Nephrol. 25 (3) (1993) 215–220.
[41] Z. Zhang, Y. Li, J. Wan, et al., Preparation of Pt(IV)-crosslinked polymer nanoparticles with an anti-detoxifying effect for enhanced anticancer therapy, Polym. Chem. 8 (15) (2017) 2410–2422, https://doi.org/10.1039/c6py02148d.
[42] S. Dhar, N. Kolishetti, S.J. Lippard, O.C. Farokhzad, Targeted delivery of a cisplatin prodrug for safer and more effective prostate cancer therapy in vivo, Proc. Natl. Acad. Sci. U. S. A. 108 (5) (2011) 1850–1855, https://doi.org/10.1073/pnas.1011379108.
[43] C.M. Fadzen, J.M. Wolfe, C.F. Cho, E.A. Chiocca, S.E. Lawler, B.L. Pentelute, Perfluoroarene-based peptide macrocycles to enhance penetration across the blood-brain barrier, J. Am. Chem. Soc. 139 (44) (2017) 15628–15631, https://doi.org/10.1021/jacs.7b09790.
[44] J. Zhou, Y. Kang, L. Chen, et al., The drug-resistance mechanisms of five platinum-based antitumor agents, Front. Pharmacol. (2020) 11, https://doi.org/10.3389/fphar.2020.00343.
[45] D. Huang, S.R. Savage, A.P. Calinawan, et al., A highly annotated database of genes associated with platinum resistance in cancer, Oncogene. 40 (46) (2021) 6395–6405, https://doi.org/10.1038/s41388-021-02055-2.
[46] X.Y. Zhang, A.A. Elfarra, Toxicity mechanism-based prodrugs: glutathione-dependent bioactivation as a strategy for anticancer prodrug design, Expert Opin. Drug Discovery 13 (9) (2018) 815–824, https://doi.org/10.1080/17460441.2018.1508207.
[47] N. Graf, S.J. Lippard, Redox activation of metal-based prodrugs as a strategy for drug delivery, Adv. Drug Deliv. Rev. 64 (11) (2012) 993–1004, https://doi.org/10.1016/j.addr.2012.01.007.
[48] E. Wexselblatt, D. Gibson, What do we know about the reduction of Pt(IV) pro-drugs?, in: Journal of Inorganic Biochemistry vol. 117, 2012, pp. 220–229, https://doi.org/10.1016/j.jinorgbio.2012.06.013.
[49] A. Nemirovski, Y. Kasherman, Y. Tzaraf, D. Gibson, Reduction of cis,trans,cis-[PtCl2(OCOCH3) 2(NH3)2] by aqueous extracts of cancer cells, J. Med. Chem. 50 (23) (2007) 5554–5556, https://doi.org/10.1021/jm070740j.
[50] F. Raynaud, D.E. Odell, L.R. Kelland, Intracellular Metabolism of the Orally Active Platinum Drug JM216: Influence of Glutathione Levels vol. 74, 1996.
[51] L. Kennedy, J.K. Sandhu, M.E. Harper, M. Cuperlovic-culf, Role of glutathione in cancer: from mechanisms to therapies, Biomolecules. 10 (10) (2020) 1–27, https://doi.org/10.3390/biom10101429.
[52] Y. Chen, J. Gu, J. Liu, et al., Dexamethasone-loaded injectable silk-polyethylene glycol hydrogel alleviates cisplatin-induced ototoxicity, Int. J. Nanomedicine 14 (2019) 4211–4227, https://doi.org/10.2147/IJN.S195336.
[53] Y. Hussain, L. Islam, H. Khan, R. Filosa, M. Aschner, S. Javed, Curcumin–cisplatin chemotherapy: a novel strategy in promoting chemotherapy efficacy and reducing side effects, Phytother. Res. 35 (12) (2021) 6514–6529, https://doi.org/10.1002/ptr.7225.
[54] I. Ruseska, A. Zimmer, Internalization mechanisms of cell-penetrating peptides, Beilstein J. Nanotechnol. 11 (2020) 101–123, https://doi.org/10.3762/bjnano.11.10.
[55] M.Z. Islam, H. Ariyama, J.M. Alam, M. Yamazaki, Entry of cell-penetrating peptide transportan 10 into a single vesicle by translocating across lipid membrane and its induced pores, Biochemistry. 53 (2) (2014) 386–396, https://doi.org/10.1021/bi401406p.
[56] R.F.C.P.A. Helderman, D.R. Löke, J. Verhoeff, et al., The temperature-dependent effectiveness of platinum-based drugs Mitomycin-C and 5-FU during Hyperthermic intraperitoneal chemotherapy (HIPEC) in colorectal Cancer cell lines, Cells. 9 (8) (2020), https://doi.org/10.3390/cells9081775.
[57] Y. Zhu, Y. Jiang, F. Meng, et al., Highly efficacious and specific anti-glioma chemotherapy by tandem nanomicelles co-functionalized with brain tumor-targeting and cell-penetrating peptides, J. Control. Release 278 (2018) 1–8, https://doi.org/10.1016/j.jconrel.2018.03.025.
[58] L. Wei, X.Y. Guo, T. Yang, M.Z. Yu, D.W. Chen, J.C. Wang, Brain tumor-targeted therapy by systemic delivery of siRNA with transferrin receptor-mediated core-shell nanoparticles, Int. J. Pharm. 510 (1) (2016) 394–405, https://doi.org/10.1016/j.ijpharm.2016.06.127.
[59] Q. Guo, Q. Zhu, T. Miao, et al., LRP1-upregulated nanoparticles for efficiently conquering the blood-brain barrier and targetedly suppressing multifocal and infiltrative brain metastases, J. Control. Release 303 (2019) 117–129, https://doi.org/10.1016/j.jconrel.2019.04.031.
[60] G. Berger, K. Grauwet, H. Zhang, et al., Anticancer activity of osmium(VI) nitrido complexes in patient-derived glioblastoma initiating cells and in vivo mouse models, Cancer Lett. 416 (2018) 138–148, https://doi.org/10.1016/j.canlet.2017.11.041.
[61] A.R. Timerbaev, Application of ICP-MS to the development of metal-based drugs and diagnostic agents: where do we stand? J. Anal. At. Spectrom. 36 (2) (2021) 254–266, https://doi.org/10.1039/d0ja00404a.
[62] Y. Koyama, Y. Matsui, Y. Shimada, M. Yoneda, Biodistribution of gold nanoparticles in mice and investigation of their possible translocation by nerve uptake around the alveolus, J. Toxicol. Sci. 40 (2) (2015) 243–249.
[63] J. Wang, J. Tao, S. Jia, M. Wang, H. Jiang, Z. Du, The protein-binding behavior of platinum anticancer drugs in blood revealed by mass spectrometry, Pharmaceuticals. 14 (2) (2021) 1–17, https://doi.org/10.3390/ph14020104.
[64] B. Neumann, S. Hösl, K. Schwab, F. Theuring, N. Jakubowski, Multiplex LA-ICP-MS bio-imaging of brain tissue of a parkinsonian mouse model stained with metal-coded affinity-tagged antibodies and coated with indium-spiked commercial inks as internal standards, J. Neurosci. Methods (2020) 334, https://doi.org/10.1016/j.jneumeth.2020.108591.
[65] M. Vojtek, E. Pinto, S. Gonçalves-Monteiro, et al., Fast and reliable ICP-MS quantification of palladium and platinum-based drugs in animal pharmacokinetic and biodistribution studies, Anal. Methods 12 (39) (2020) 4806–4812, https://doi.org/10.1039/d0ay01328e.
[66] T. Zhang, S. Cai, W.C. Forrest, E. Mohr, Q. Yang, M.L. Forrest, Development and validation of an inductively coupled plasma mass spectrometry (ICP-MS) method

for quantitative analysis of platinum in plasma, urine, and tissues, Appl. Spectrosc. 70 (9) (2016) 1529–1536, https://doi.org/10.1177/0003702816662607.
[67] E. White, A. Bienemann, J. Pugh, et al., An evaluation of the safety and feasibility of convection-enhanced delivery of carboplatin into the white matter as a potential treatment for high-grade glioma, J. Neuro-Oncol. 108 (1) (2012) 77–88, https://doi.org/10.1007/s11060-012-0833-4.
[68] M. Dehnhardt, M.V. Zoriy, Z. Khan, et al., Element distribution is altered in a zone surrounding human glioblastoma multiforme, J. Trace Elem. Med. Biol. 22 (1) (2008) 17–23, https://doi.org/10.1016/j.jtemb.2007.08.002.
[69] A.L. Brown, M.P. Kai, A.N. DuRoss, G. Sahay, C. Sun, Biodistribution and toxicity of micellar platinum nanoparticles in mice via intravenous administration, Nanomaterials. 8 (6) (2018), https://doi.org/10.3390/nano8060410.
[70] J. Li, A. Pant, C.F. Chin, et al., In vivo biodistribution of platinum-based drugs encapsulated into multi-walled carbon nanotubes, Nanomedicine. 10 (7) (2014) 1465–1475, https://doi.org/10.1016/j.nano.2014.01.004.
[71] G. Thiabaud, G. He, S. Sen, et al., Oxaliplatin Pt(IV) prodrugs conjugated to gadolinium-texaphyrin as potential antitumor agents, Proc. Natl. Acad. Sci. 117 (13) (2020) 7021–7029, https://doi.org/10.1073/PNAS.1914911117.
[72] Q. Chang, O.I. Ornatsky, I. Siddiqui, R. Straus, V.I. Baranov, D.W. Hedley, Biodistribution of cisplatin revealed by imaging mass cytometry identifies extensive collagen binding in tumor and normal tissues, Sci. Rep. (2016) 6, https://doi.org/10.1038/srep36641.
[73] K. Namikawa, M. Asakura, T. Minami, Y. Okazaki, E. Kadota, S. Hashimoto, Toxicity of Cisplatin to the Central Nervous System of Male Rabbits vol. 223, 2000.
[74] E.E.M. Brouwers, A.D.R. Huitema, J.H. Beijnen, J.H.M. Schellens, Long-term platinum retention after treatment with cisplatin and oxaliplatin, BMC Clin. Pharmacol. (2008) 8, https://doi.org/10.1186/1472-6904-8-7.
[75] A. Ozkok, C.L. Edelstein, Pathophysiology of cisplatin-induced acute kidney injury, Biomed. Res. Int. 2014 (2014), https://doi.org/10.1155/2014/967826.
[76] A.M. Breglio, A.E. Rusheen, E.D. Shide, et al., Cisplatin is retained in the cochlea indefinitely following chemotherapy, Nat. Commun. 8 (1) (2017), https://doi.org/10.1038/s41467-017-01837-1.
[77] X. Li, Y. Liu, H. Tian, Current developments in Pt(IV) prodrugs conjugated with bioactive ligands, Bioinorg. Chem. Appl. 2018 (2018), https://doi.org/10.1155/2018/8276139.
[78] L. Ma, R. Ma, Y. Wang, et al., Chalcoplatin, a dual-targeting and p53 activator-containing anticancer platinum(iv) prodrug with unique mode of action, Chem. Commun. 51 (29) (2015) 6301–6304, https://doi.org/10.1039/c4cc10409a.
[79] C. Yu, Z. Wang, Z. Sun, et al., Platinum-based combination therapy: molecular rationale, current clinical uses, and future perspectives, J. Med. Chem. 63 (22) (2020) 13397–13412, https://doi.org/10.1021/acs.jmedchem.0c00950.